RSC Advances

PAPER

View Article Online
View Journal | View Issue

Cite this: *RSC Adv.*, 2020, **10**, 23899

Green synthesis of ZnO nanoparticles using orange fruit peel extract for antibacterial activities

Tu Uyen Doan Thi,†[ab] Trung Thoai Nguyen,†[ab] Y Dang Thi,[c] Kieu Hanh Ta Thi,[ab] Bach Thang Phan[bc] and Kim Ngoc Pham *[abc]

Received 4th June 2020
Accepted 18th June 2020

DOI: 10.1039/d0ra04926c

rsc.li/rsc-advances

This paper presents an efficient, environmentally friendly, and simple approach for the green synthesis of ZnO nanoparticles (ZnO NPs) using orange fruit peel extract. This approach aims to both minimize the use of toxic chemicals in nanoparticle fabrication and enhance the antibacterial activity and biomedical applications of ZnO nanoparticles. In this work, an aqueous extract of orange peel was used as the biological reduction agent for the synthesis of ZnO NPs from zinc acetate dihydrate. It was found that the size and morphology of the ZnO NPs significantly depended on physicochemical parameters such as the annealing temperature and pH during NP synthesis. The ZnO NPs exhibited strong antibacterial activity toward *Escherichia coli* (*E. coli*) and *Staphylococcus aureus* (*S. aureus*) without UV illumination at an NP concentration of 0.025 mg mL^{-1} after 8 h of incubation. In particular, the bactericidal activity towards *S. aureus* varied extensively with the synthesis parameters. This study presents an efficient green synthesis route for ZnO NPs with a wide range of potential applications, especially in the biomedical field.

1. Introduction

Since organic antibacterial agents are sensitive to processing conditions such as high temperature and pressure, in recent years, inorganic antibacterial agents have become a new area of research interest for the control of microbes.[1] Antibacterial activity is still strong even at low concentrations of inorganic materials, particularly metal oxides. Compared to organic antibacterial agents, the main advantages of inorganic antibacterial agents are their good stability at high temperatures and pressures and their long shelf-life.[2] Currently, the most widely used inorganic antibacterial materials are metallic nanoparticles and metal oxide nanoparticles.[1]

Zinc oxide is a semiconducting inorganic material with three different crystal structures: wurtzite, zinc blende, and rocksalt. At ambient conditions, the structure of wurtzite is thermodynamically stable, with every zinc atom being tetrahedrally coordinated with four oxygen atoms.[3] With a wide band gap of 3.1–3.3 eV,[4] zinc oxide has great potential for application in many fields, such as biosensors, cosmetics, drug carriers, and antibacterial agents.[5,6] ZnO can be synthesized by many different methods, such as sol–gel processing, homogeneous precipitation, mechanical milling, organometallic synthesis, the microwave method, spray pyrolysis, thermal evaporation, and mechanochemical synthesis.[7] However, these kinds of methods usually use organic solvents and toxic reducing agents, the majority of which are highly reactive and harmful to the environment. Therefore, in order to minimize the impact on the environment, green synthesis processes have been used to synthesize ZnO nanoparticles (ZnO NPs). Green synthesis is a method to produce nanoparticles using microorganisms and plants with biomedical applications. This method has many advantages, such as environmental friendliness, cost-effectiveness, biocompatibility, and safety. Additionally, many studies have proved that ZnO NPs made using green synthesis processes have strong antibacterial properties.

Recently, ZnO NPs have been successfully synthesized using extracts from plants. D. Xu *et al.*[8] synthesized ZnO NPs using *Citrus sinensis* peel extract and compared with commercial ZnO NPs and then applied as nanocoatings on fresh strawberries to evaluate the preservation effect. The high antibacterial and antifungal activities of ZnO NPs improve potential in food packaging application. P. A. Luque *et al.*[9] has addressed the influence of different amounts of *Citrus sinensis* extract on the size and shape homogeneity of ZnO NPs. Besides, photocatalytic degradation of methylene blue (MB) under UV light of ZnO NPs presented a better rate than commercial ZnO NPs. O. J. Nava *et al.*[10] found that ZnO NPs exhibited various size and shape distribution with using *Lycopersicon esculentum* (tomato), *Citrus sinensis* (orange), *Citrus paradisi* (grapefruit) and *Citrus aurantifolia* (lemon) extracts. Most ZnO samples exhibited degradation rates of MB under UV light at 180 min of around 97%. H. J. Malmiri *et al.*[11] evaluated of three different green fabrication methods including microwave irradiation, autoclave

[a]*Faculty of Materials Science and Technology, University of Science, Hochiminh City, Vietnam. E-mail: phamkngoc@hcmus.edu.vn*
[b]*Vietnam National University, Hochiminh City, Vietnam*
[c]*Center of Innovative Materials and Architectures, Hochiminh City, Vietnam*
† These authors contributed equally to this work.

and conventional heating for ZnO synthesis using Pelargonium zonale leaf extract. Although different size and antioxidant activities, all the formed ZnO NPs had bactericidal effects against to the both Gram negative and Gram positive bacteria strains. S. Jafarirad *et al.*[12] also used both microwave irradiation and conventional heating to synthesis ZnO NPs from *Rosa canina* fruit extract. The antibacterial activities of ZnO NPs with several bacteria such as *Listeria monocytogenes*, *E. coli* and *Salmonella typhimurium* were investigated. K. S. Ahmad[13] synthesized silver doped ZnO NPs *via* hydro-thermal route utilizing *Prunus cerasifera* leaf extract and it found that ZnO : Ag NPs to be an efficient nanophotocatalyst against bromocresol green and bromophenol blue in direct solar irradiance. ZnO–Ag nanocomposite was also synthesized using *Thymus vulgaris* leaf extract and showed antimicrobial activity against food-borne pathogen, biocompatibility and solar photocatalysis.[14] G. Madhumitha *et al.*[15] used *Aegle marmelos* leaf extract to synthesis ZnO NPs for antimicrobial activity against *A. niger*. Using *Tecoma castanifolia* leaf extract,[16] ZnO NPs were observed an excellent antibacterial and anticancer to lead its effective application in biomedical and nano-drug delivery systems. From *Citrus aurantifolia* extracts and different concentrations of zinc acetate,[17] ZnO NPs in range size of 50–200 nm were synthesized by sol–gel method. Using different volume of lemon juice, ZnO NPs were synthesized and showed the good photocatalytic activity for degradation of methyl orange, methyl red and methylene blue solutions.[18] Ramesh *et al.* successfully synthesized ZnO NPs nanoparticles with sizes of 20–30 nm from *Solanum nigrum* leaf extract. The resulting ZnO NPs had a band energy of 3.38 eV with strong bactericidal ability against Gram-positive bacteria (*S. aureus*) and Gram-negative bacteria (*S. paratyphi*, *V. cholerae*, *E. coli*).[19] Joel *et al.* compared the bactericidal properties of ZnO NPs synthesized from *Phyllanthus embilica* (forest tamarind) stem extract with those of chemically synthesized ZnO NPs.[7] These authors found that, compared to the ZnO NPs synthesized by chemical methods, the green-synthesized ZnO NPs showed stronger bactericidal properties on Gram-negative bacteria (*Salmonella typhi* and *Klebsiella pneumoniae*). The sizes of the synthesized nanoparticles ranged from 15–25 nm and the nanoparticles had an E_g of 2.8 eV. Moreover, Ogunyemi *et al.* synthesized ZnO NPs using extract of chamomile flower (*Matricaria chamomilla* L.), olive leaf (*Olea europaea*) and red tomato fruit (*Lycopersicon esculentum* M.).[20] Overall, the results demonstrated that the growth, biofilm formation, swimming motility, and cell membrane of Xoo strain GZ 0003 were significantly affected by the synthesized ZnO NPs. Furthermore, Awwad *et al.* synthesized ZnO NPs using *Ailanthus altissima* fruit extracts and found that the nanoparticles exhibited highly efficient antibacterial activity against *E. coli* and *S. aureus*.[21] The above studies show that the green synthesis of ZnO NPs is simple, environmentally friendly (by avoiding the use of toxic chemicals), and cost-effective. Moreover, the synthesized ZnO NPs have outstanding physical and chemical properties and wide applicability.

On the other hand, in the previous reports of ZnO material synthesis by physical and chemical route, various factors to improve the characterization of ZnO NPs include aging time, annealing temperature, doping element, quenching effect, pH value⋯[22] Using simple combustion method, influence of pH from 5 to 11 greatly effects on morphology and electrical properties of ZnO NPs, in which the ideal pH value for photocatalytic degradation towards direct red dye is at 9. P. S. Kumar *et al.*[23] reported the influence of pH on growth and orientation of ZnO nanorods *via* aqueous solution process. With the pH ranged from 6–8, ZnO rods exhibited perfect wurtzite hexagonal shape and diameters from 300 nm to 1 μm. Simillarly, ZnO nanorods synthesized from chemical bath deposition and their morphology, surface topography and furface roughness were affected by different pH solution from 9.5 to 11.5. In addition, influence of annealing temperature from 100–600 °C on ZnO nanostructures were studied by Manoj Pudukudy *et al.*[24] *via* a simple precipitation route. Under temperature @300 °C, the ZnO morphology was more-less spherical shape while temperature larger than 300 °C, the ZnO was elongation of quasi-spherical or nanorod-like morphology. The photocatalytic activity of MB was highest at 600 °C and highly reusable. To study both the influence of pH and annealing, K. Shingange *et al.*[25] reported 0D to 3D ZnO nanostructures and corresponding properties by using microwave assisted hydrothermal. The morphology of ZnO nanomaterials prepared at pH from 7–13 varied from particles, spheres, flowers to roses at as-prepared samples and from particles, flowers and platelets at 400 °C annealed samples. Among synthesized parameters of ZnO material, annealing temperature and pH values are reported as the most important parameters to strongly affect the morphology and properties of ZnO NPs.

Orange fruit is one of the most productive fruit in the world. Orange fruit peel, as the main by-product of citrus, is rich in a variety of natural anti-oxidants. Therefore, the extract of orange peel is considered to be used as a stabilizer to prepare ZnO NPs. However, ZnO NPs green synthesis based on extracts of orange fruit peel are not studied fully. Particularly, the influence of pH value and annealing temperature on morphology and properties of ZnO NPs by green synthesis till lacks of understanding. Herein, ZnO NPs were synthesized *via* a green process using orange fruit peel extract and investigated the influence of pH and annealing temperature on morphology and antibacterial activities. The morphology and structure of the ZnO NPs were characterized using a transmission electron microscope (TEM), X-ray diffraction (XRD), and Fourier-transform infrared spectroscopy (FTIR). Furthermore, the antibacterial activity of ZnO nanofluids was tested against *S. aureus* and *E. coli via* a broth dilution method. In order to optimize the bactericidal activity of the ZnO NPs, measurements were carried out with various types of ZnO NPs fabricated at different annealing temperatures and pH levels.

2. Materials and methods

2.1. Materials

Materials used: (1) zinc nitrate ($Zn(NO_3)_2 \cdot 6H_2O$) as the zinc precursor (Sigma-Aldrich); (2) orange peel, chosen for its high content of desired organic compounds in relation to market availability; (3) de-ionized water as the synthesis medium.

2.2. Preparation of peel extracts

In order to obtain the extracts, orange fruits were washed and dried before being peeled as thinly as possible. The peel was then placed in a food drier for 12 h until completely dry and was then ground into a moderately fine powder. Afterwards, 1 g of the powder was placed in different glass containers with 50 mL of de-ionized water in each container and was stirred for 3 hours. Once macerated, each mixture was placed in a water bath at 60 °C for 60 minutes. Finally, the mixtures were filtered and the resulting extracts were stored in argon atmosphere for later use.

2.3. Synthesis of ZnO nanoparticles

The ZnO NPs were synthesized by mixing 2 g of zinc nitrate with 42.5 mL of each of the extracts. These mixtures were then stirred for 60 minutes and then placed in a water bath at 60 °C for 60 minutes. Subsequently, the mixtures were dried at 150 °C and then heat-treated at 400 °C for 1 hour. A schematic of the synthesis process of the ZnO NPs is shown in Fig. 1.

Fig. 2 presents a possible reaction mechanism for the synthesis process of ZnO using orange peel extract in which ligation takes place between the functional components of the orange peel and the zinc precursor. The organic substances (Flavonoid, Limonoid, Carotenoids) in orange peel extract act as ligand agents. These hydroxyl aromatic ring groups, one of the extract components, form complex ligands with zinc ions. Through the process of nucleation, shaping, nanoparticles are stabilized and formed. The mixture of organic solution is then decomposed directly when calcination at 400 °C resulting in the release of ZnO nanoparticles[9,26].

2.4. Analysis of ZnO nanoparticles

X-ray diffraction studies of the dried ZnO NPs were carried out using a Siemens D5000 instrument (Bruker, Germany) in order to characterize the crystallinity of the nanoparticles. The vibrational peaks of the ZnO NPs were observed by FTIR analysis using a Tensor 27 instrument (Bruker). Thermogravimetric analysis (TGA) was performed using a Q500 instrument (TA Instruments) in order to measure the weight loss of the ZnONP powder as a function of temperature in the range from room temperature (RT) to 800 °C. The morphology and particle size of the ZnO NPs were characterized using a JEOL TEM (Hitachi, Ltd., Tokyo, Japan).

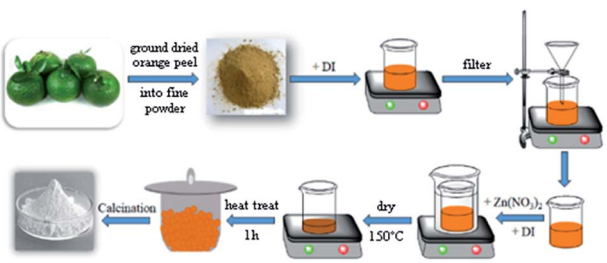

Fig. 1 Schematic diagram of the green synthesis of ZnO nanoparticles (ZnO NPs).

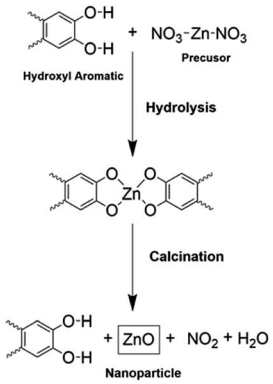

Fig. 2 The chemical mechanism of ZnO nanoparticle formation.

2.5. Antibacterial activities

Two types of bacteria, *S. aureus* and *E. coli*, were used to test the antibacterial activity of the ZnO NPs *via* a broth dilution method. Bacterial strains stored in Trypticase soy agar (TSA) in order to proliferate at 37 °C for 18–24 h. The bacterial proliferation was done twice. Then, bacterial strains would be use to conduct the tests. A total bacteria concentration of 10^6 CFU mL^{-1} was used for the experiments, which was determined by diluting the bacterial suspension and adjusting its turbidity using 0.5 McFarland standards. The bacterial suspension will be exposed to the ZnO NPs solution (0.025 mg mL^{-1}) for 8 hours without UV light. The number of colonies was calculated to estimate the growth rate of the bacteria before and after the incubation with the ZnO NPs solution. The agar plate count method was used to determine the number of living cells. Then, the antibacterial activity was calculated using the following formula:

$$\text{Antibacterial activity } (\%) = [(a - b)/a] \times 100$$

where a is the initial number of cells and b is the number of living cells.

3. Results and discussion

3.1. Influence of annealing temperature

In order to investigate the influence of the annealing temperature on the physical and chemical properties of the ZnO NPs, powder samples were annealed at temperatures of 300 to 900 °C for 1 h. The appearances of ZnONP powder for the as-prepared samples and for samples annealed at various temperatures are shown in Fig. 3.

All of the ZnONP powders had a fluffy appearance but had different colors. The as-prepared sample was dark orange since the orange-peel extract had not been totally removed. However, the annealed samples had lighter colors due to the decomposition of organic substances. The higher the annealing temperature, the lighter the powder color.

Transmission electron microscope images of the as-prepared ZnO NPs and the ZnO NPs annealed at various temperatures are shown in Fig. 4. The as-prepared sample (Fig. 4a) exhibited

Fig. 3 Photographs of ZnONP powders with different annealing temperatures.

relatively small spherical particles (10–20 nm) which were coagulated in large clusters on a matrix of residual organic material from the reduction agents. In the samples annealed at 400 °C and 700 °C, the particle sizes were randomly distributed and ranged from 35–60 nm and 70–100 nm, respectively. For an annealing temperature of 900 °C, the particle size increased intensively in the range of 200–230 nm. Moreover, it was found that the morphology and size of the ZnO NPs depended on the annealing temperature, which is similar to the findings of a previous report.[27] Specifically, with increasing annealing temperature, the particle size tended to increase and shape larger particles due to crystal growth.[28]

The XRD patterns of ZnO NPs with various annealing temperatures are shown in Fig. 5a. The as-prepared sample showed poor crystalline structure due to low-temperature synthesis. The other samples exhibited preferred diffraction peaks at $2\theta \approx 31.77°$, 34.42°, and 36.25°, corresponding to lattice planes of (100), (002), and (101), respectively, while the other peaks at $2\theta \approx 47.53°$, 56.60°, 62.86°, 66.38°, 67.96°, and 69.10°, corresponding to lattice planes of (102), (110), (103), (200), (112), and (201), respectively (JCPDS: 36-1451).[29] These observations confirmed that the ZnO NPs exhibited a hexagonal wurtzite structure. When the annealing temperature increased from 300–900 °C, the intensity of the diffraction peaks and crystalline size both increased. The crystalline size (D) was calculated using the Scherrer equation: $D = (0.9 \times \lambda)/(\beta \times \cos\theta)$ (Å), where λ is the wavelength Cu Kα 1.5406 Å, β is the full width at half maximum (rad), and θ is the diffraction angle (degrees). The smallest average crystalline size of around 12 nm was observed for the as-prepared sample and the average crystalline size increased successively for higher annealing temperatures; average crystalline temperatures of 22, 24, 40, 44, 55, 70, and

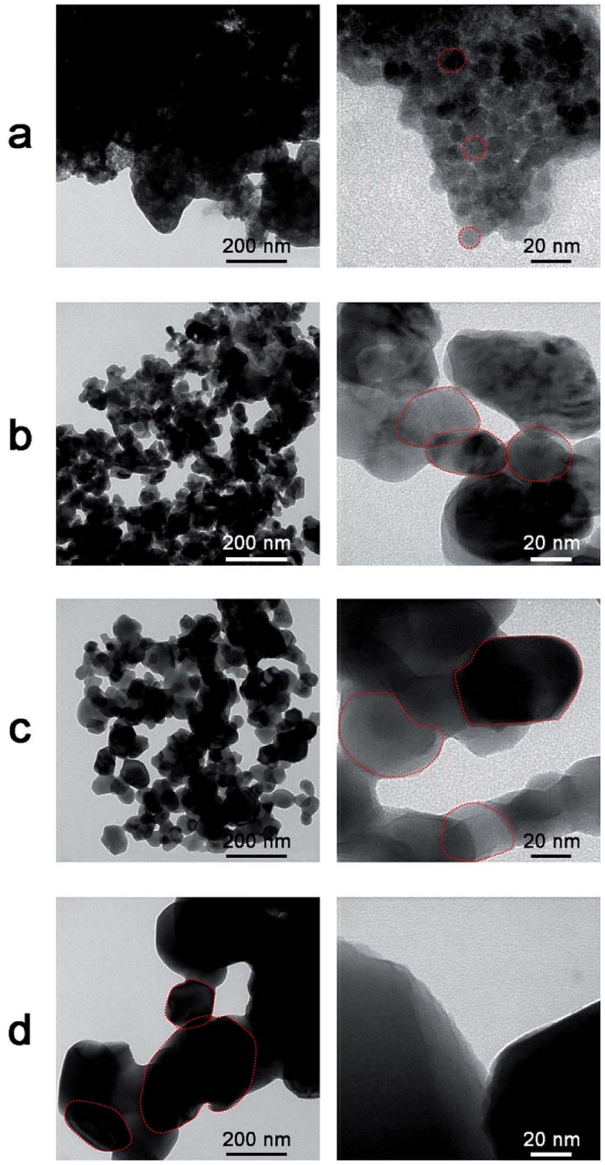

Fig. 4 Transmission electron microscope images of ZnO NPs with different annealing temperatures. (a) shows the as-prepared sample and (b), (c), and (d) show samples annealed at 400, 700, and 900 °C, respectively.

95 nm were observed for annealing temperatures of 300, 400, 500, 600, 700, 800, and 900 °C, respectively. This increase in crystalline size can be attributed to the fact that the thermal energy during annealing caused the particles to become re-oriented and reduced the number of defects in grain boundaries.[30] The particle size determined based on the XRD results is consistent with the results of the TEM analysis.

The FTIR spectra of the ZnO NPs for various annealing temperatures and orange peel extract are shown in Fig. 5b and c. The as-prepared samples and the samples annealed at temperatures between 300 and 900 °C presented vibration bands at around 450 cm^{-1}, which are assigned to the stretching vibration of Zn–O bonding. The peak at 1640 cm^{-1} in the FTIR spectrum of orange peel extract represented the stretching

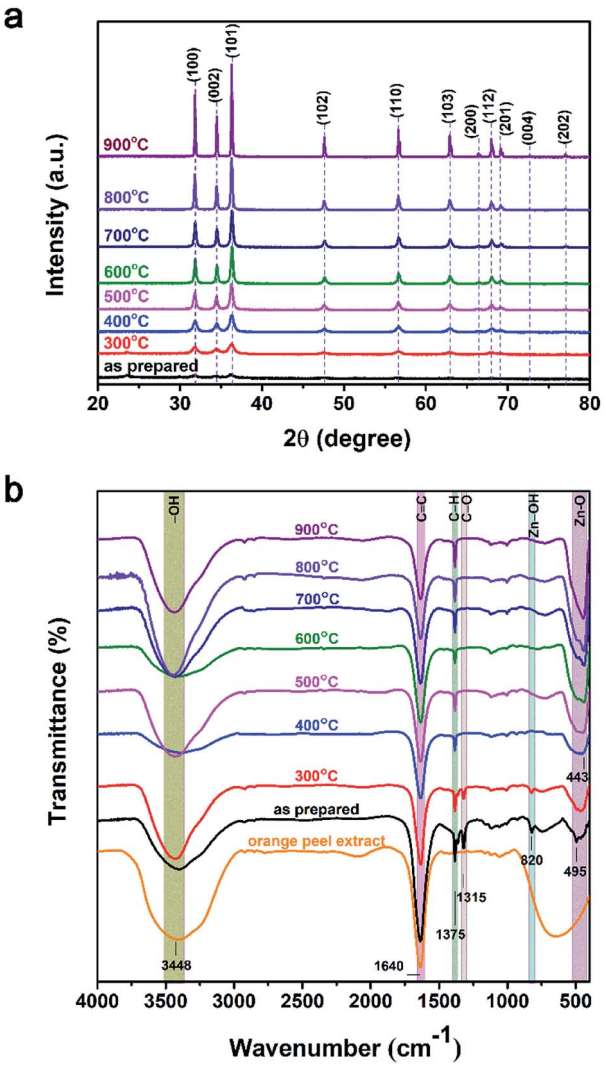

Fig. 5 The results of the synthesized ZnO NPs for as-prepared samples and for samples annealed at temperatures of 300–900 °C. (a) X-ray diffraction pattern. (b) Fourier-transform infrared spectroscopy.

bands of C=C and C=O functional groups.[8,31] In the FTIR spectra of ZnO NPs synthesized at different temperatures is also observed the similar peak at this position. It may be due to the annealing time of ZnO NPs only for one hour, therefore, the organic functional groups C=C and C=O at 1640 cm^{-1} have not been completely decomposed. This leads to the present of this vibrational peak existing in our the sample.[32] Besides, the presence of a broad peak at 3500 cm^{-1} related to the absorption of CO_2 and molecular water on the surface of nanoparticles.[33] In the as-prepared samples and the samples annealed at a temperature of 300 °C, there were additional low-intensity peaks at 820 and 1316 cm^{-1}, which may be due to vibrations of residual organic extract in the nanoparticles. At higher annealing temperatures, the intensity of these peaks gradually decreased. Furthermore, with increasing annealing temperature, the intensity of the Zn–O absorption peak increased and the peak shifted to lower wavenumbers (higher energies). This can be explained by the improvement of the crystalline structure of the ZnO NPs with increasing annealing temperature as indicated by the XRD results.

The thermal stability of the ZnO NPs provides information on their physical characteristics and the components present. The TGA spectra up to 800 °C and the weight loss at 500 °C are shown in Fig. 6a and b, respectively. The results indicate that the as-prepared sample and the sample annealed at 300 °C exhibited an abrupt weight loss, whereas the other samples were nearly unchanged. For the as-prepared sample, an initial weight loss was observed at 100 °C due to the loss of moisture and organic substances in the sample. Between 100 and 400 °C, the residual precursors continued to be removed and released as CO_2. After 400 °C, the weight loss appeared to stabilize, indicating that impurities had been almost entirely eliminated by this temperature. In the samples annealed at temperatures of 400–900 °C, the weight loss was minor and was mainly due to the degradation of moisture and CO_2 absorption. The weight loss of the ZnO NPs powder at 500 °C is shown in Fig. 6b. The largest weight loss of 35.7% was observed in the as-prepared sample, and the weight loss decreased continuously with increasing annealing temperature. A good thermal stability was

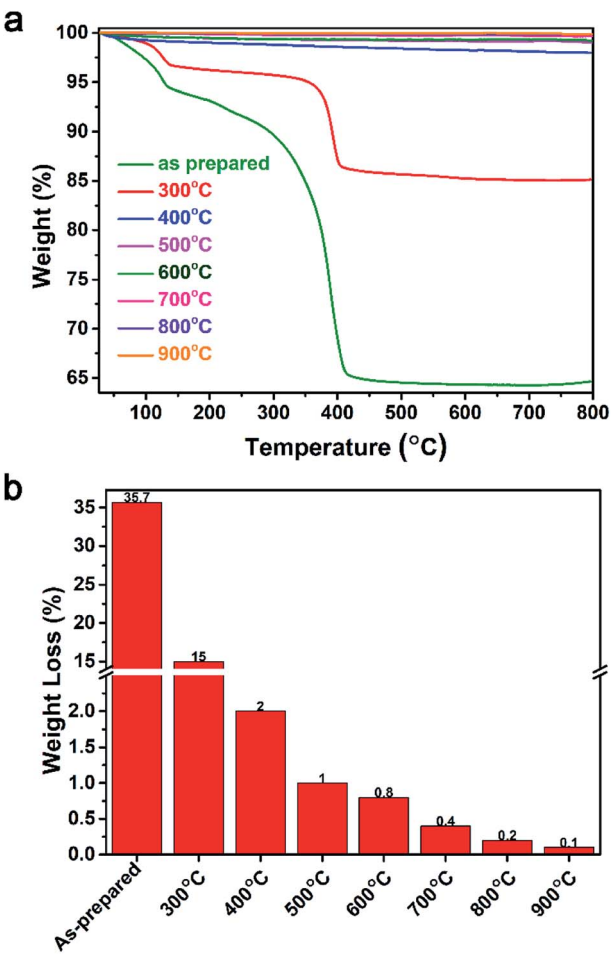

Fig. 6 Thermogravimetric analysis of the synthesized ZnO NPs for as-prepared samples and for samples annealed at temperatures of 300–900 °C. (a) Thermogravimetric spectra. (b) Weight loss at 500 °C.

observed for annealing temperatures of 500–900 °C, with weight losses lower than 1.0%.

As shown in Fig. 7, all of the ZnO NPs samples showed a high performance in sterilizing *E. coli* bacteria, with bactericidal rates of 99.96 to 99.99%, whereas the bactericidal rates for *S. aureus* varied with treatment temperature. The as-prepared sample had the highest bactericidal rate against *S. aureus*, namely 94.29%. Since the average particle size of the as-prepared sample was the smallest, this observation is consistent with the assumption that smaller ZnO NPs have better antibacterial activity.[34] The samples annealed at 400 °C had the lowest bactericidal rate (89.41%) and the bactericidal rate increased with increasing annealing temperature (700 °C: 91.77%; 900 °C: 98.14%).

The differences in the antibacterial effects of the ZnO NPs can be explained as follows. The as-prepared sample still contained orange-peel extract, while in the sample annealed at 400 °C, the orange-peel extract had evaporated. Hence, the as-prepared sample had more bactericidal ability than the 400 °C sample. This can also be explained by the results of Shetty *et al.*,[35] who attributed the antibacterial ability of orange-peel extract to aromatic and saturated organic molecules such as tannins, saponins, phenolic compounds, essential oils, and flavonoids, which have biological properties and are able to form complexes with cellular proteins that inhibit bacterial growth and disrupt of bacterial cell membranes. In the present study, the ZnO NPs samples annealed at 700 °C and 900 °C, respectively, no longer contained orange-peel extract, and therefore, based on the findings of Zhang *et al.*,[36] the bactericidal ability of these samples can be concluded to be due to the presence of reactive oxygen species (ROS). The ZnO NPs interacted with the bacterial cell membrane or entered into the bacterial cell through bacterial transport channels. The presence of ZnO NPs creates ROS—specifically H_2O_2, $OH^{\bullet}$, or O_2-radicals—that interacted with the cell membrane, causing oxygen to react with cysteinyl protein and iron inside the cells and thus leading to damage to the bacterial DNA and cell walls.

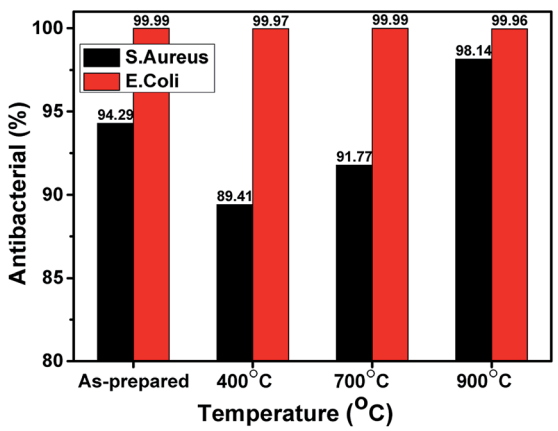

Fig. 7 The bactericidal rates of the ZnO NPs toward *E. coli* and *S. aureus* for the as-prepared samples and for samples with various annealing temperatures.

3.2. Influence of pH parameter

Several recent studies have suggested that pH affects the size and bactericidal properties of ZnO NPs synthesized by different processes. For example, Chithra *et al.* investigated the effects of pH on ZnO NPs prepared by chemical precipitation.[37] The results demonstrated that the pH value influenced the crystal size and optical properties of the synthesized ZnO nanoparticles. Furthermore, Padalia *et al.* studied the effect of pH on the formation of ZnO NPs synthesized using an aqueous extract of *Salvadora oleoides* leaf.[38] The results showed that the pH significantly affected some parameters but did not affect other parameters. Specifically, pH was found to affect the size and antibacterial activity of the ZnO NPs nanoparticles. However, the ZnO NPs still performed well as antibacterial agents. Based on previous studies, in this work, the morphology and antibacterial activity of the ZnO NPs synthesized at various pH values were investigated and compared in terms of bactericidal performance.

The appearances of the ZnONP powders synthesized at various pH values are shown in Fig. 8. As shown in the figure, the colors of the powders varied for different pH values. The powders synthesized at pH values of 4.0, 6.0, and 9.0 had an ivory color, the powders synthesized at pH values of 7.0 and 8.0 had a burnt black color, and the powders synthesized at pH values of 10 and 11 had a white color.

Transmission electron microscope images of ZnO NPs synthesized at various pH values are shown in Fig. 9. The particle size and coagulation changed significantly in higher pH conditions. For pH values of 4.0 (Fig. 9a) and 6.0 (Fig. 9b), the particles were spherical-like shape, and were distorted with distinct grain boundaries and low coagulation. In pH = 6, the particle size was in 10–20 nm range and relative seperation.

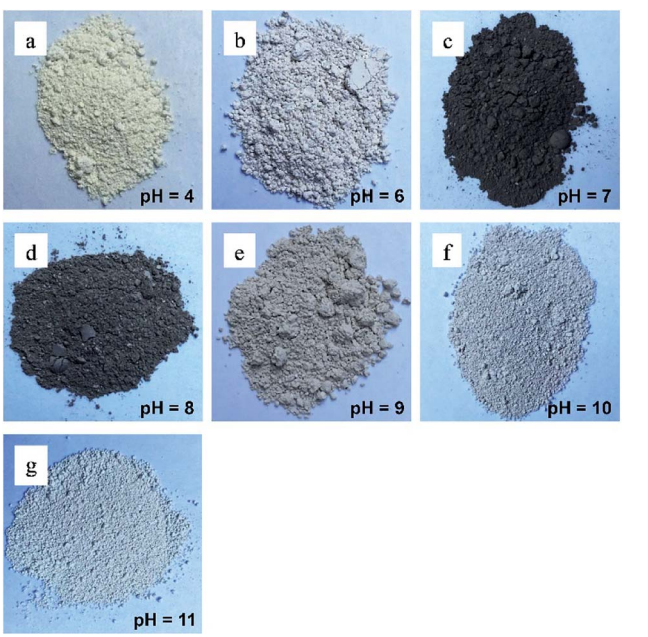

Fig. 8 Photographs of ZnONP powders synthesized at different pH values.

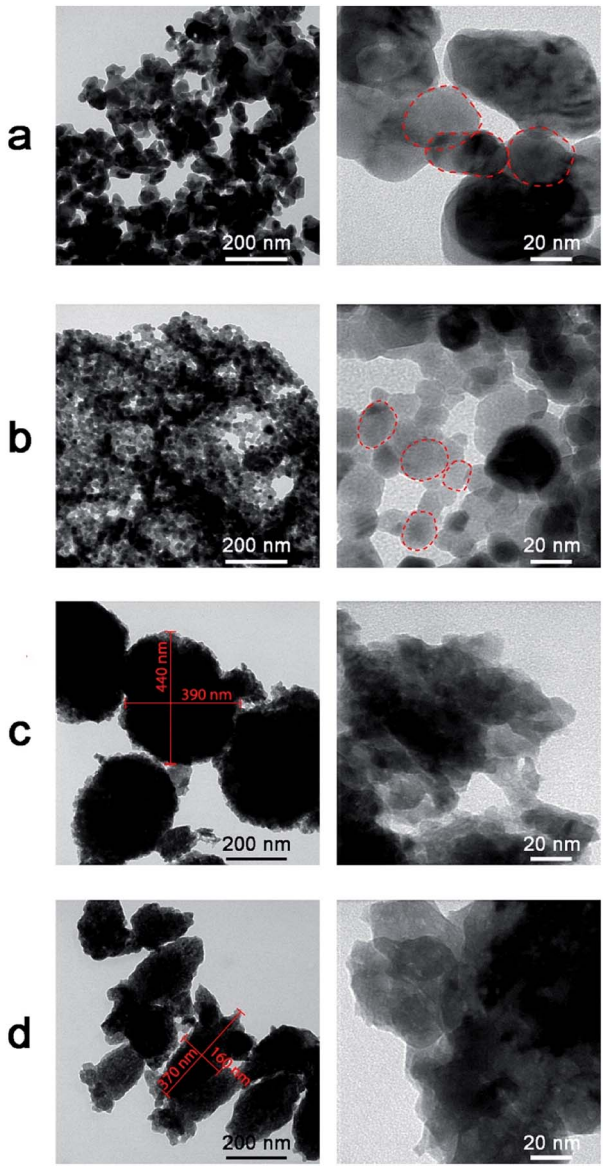

Fig. 9 Transmission electron microscope images of ZnO NPs synthesized at different pH values. (a) pH = 4. (b) pH = 6. (c) pH = 8. (d) pH = 10.

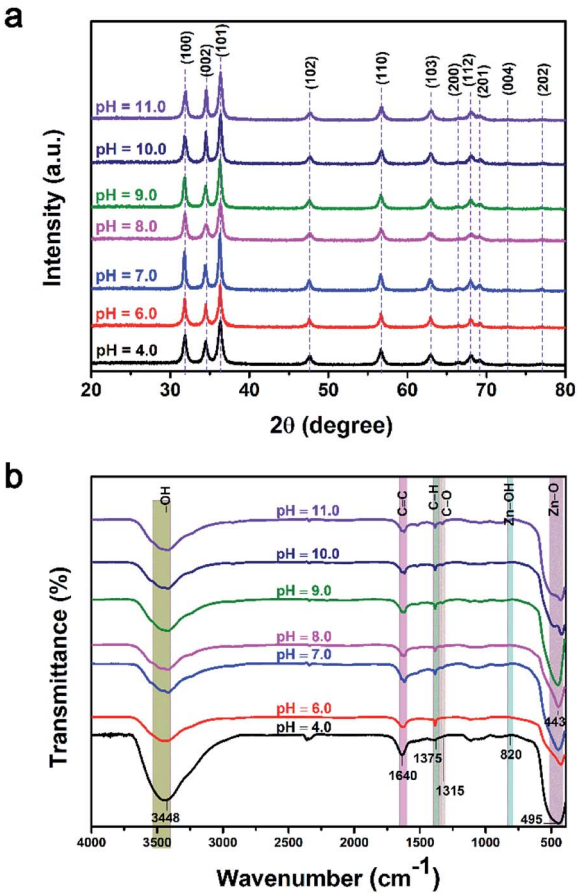

Fig. 10 (a) X-ray diffraction patterns and (b) Fourier-transform infrared spectroscopy spectra of ZnO NPs synthesized at different pH values.

Meanwhile, for a pH of 8.0 (Fig. 9c), the particles had a variable shape and were coagulated in large clusters around 400 nm in size with indistinct grain boundaries. For a pH of 10.0 (Fig. 9d), the particles were coagulated into large blocks with lengths of ~370 nm and widths of ~160 nm. This result was similar to the previous reports, in which the pH value had a strong influence on the size, morphology and properties of ZnO nanorods.[24,25]

Fig. 10a shows the XRD patterns of the ZnO NPs synthesized at various pH values. All of the samples exhibited characteristic diffraction peaks of the hexagonal wurtzite structure, in which the (101) plane has the highest intensity. The intensity of crystallization was not significantly different between the samples. For pH values of 10 and 11, the (002) plane developed similarly to the (100) plane. As shown in the figure, the crystalline size changed insignificantly and did not follow any order between the different pH treatments. The majority of crystalline sizes were smaller than 30 nm. The largest crystal size of about 39.7 nm was observed for a pH of 6.

As shown in Fig. 10b, the organic functional groups of the orange peel still appeared in all samples, however with low intensity, such as the C–O peak at 1350 cm^{-1} and the Zn–OH peak at 820 cm^{-1}. The intensity of the O–H band at 3348 cm^{-1} clearly decreased with increasing pH value. The main feature of all samples was the distinct appearance of the oscillation peaks of ZnO.

Fig. 11 shows the results of the bactericidal activity of the ZnO NPs towards *S. aureus* and *E. coli*. All samples performed excellently in sterilizing *E. coli*, with bactericidal rates of 99.97 to 99.99%. However, bactericidal ability against *S. aureus* varied for different pH values. The lowest bactericidal rate (89.41%) was obtained for a pH of 4, while the highest was obtained for a pH of 10.00 (98.43%). Recently, it has been reported that ZnO NPs are capable of producing ROS in water suspensions[39] and that the ROS produced by ZnO NPs are responsible for their inhibitory effect on the growth of bacteria[40] and fungi.[41] The results shown in Fig. 11 suggest that, when the synthesis pH increased, the ability of ZnO NPs to form ROS increased accordingly, which led to the enhancement of bactericidal activity. The pH = 8 sample had the bactericidal rate on *S.*

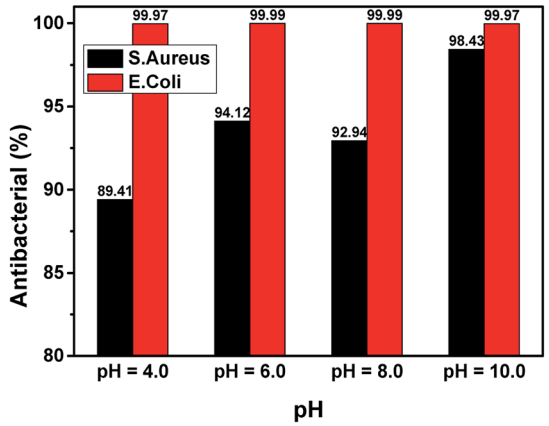

Fig. 11 The bactericidal rates of ZnO NPs synthesized at different pH values.

aureus lower than the pH = 6 sample. This may be due to the fact that the change in the nanoparticle structure for the sample synthesized at a pH of 8 affected the formation of ROS roots[40] and thus increased the bactericidal rate of the nanoparticles.

4. Conclusion and outlook

In this study, we successfully synthesized ZnO NPs by using a green synthesis method using orange-peel extract as the reducing agent. The annealing temperature and synthesis pH were found to have a significant influence on the microstructural features, morphology, and bactericidal activity toward *E. coli* and *S. aureus* of the ZnO NPs. Without UV light, the bactericidal rate towards *E. coli* was over 99.9% for all samples, while the bactericidal rate towards *S. aureus* varied in the relatively wide range of 89–98% among the samples. It is concluded that the ROS mechanism is responsible for the bactericidal activity of the ZnO NPs *via* interaction with the cell membrane and consequent damage to DNA and the cell walls. This research provides a simple and environmentally friendly method for the green synthesis of ZnO NPs using fruit peel which has the potential to reduce the use of toxic chemicals and the cost of the production of nanoparticles.

Conflicts of interest

The authors declare no conflict of interest.

Acknowledgements

This work was supported by Vietnam National Foundation for Science and Technology Development (NAFOSTED) under grant number: 103.02-2018.67.

References

1 J. Sawai, Quantitative evaluation of antibacterial activities of metallic oxide powders (ZnO , MgO and CaO) by conductimetric assay, *J. Microbiol. Methods*, 2003, **54**(2), 177–182.
2 P. Taylor, *et al.*, Synthesis, antibacterial activity, antibacterial mechanism and food applications of ZnO nanoparticles: a review, *Food Addit. Contam., Part A*, 2013, **31**(2), 1–14.
3 S. B. Kulkarni, U. M. Patil, R. R. Salunkhe, S. S. Joshi and C. D. Lokhande, Temperature impact on morphological evolution of ZnO and its consequent effect on physico-chemical properties, *J. Alloys Compd.*, 2011, **509**(8), 3486–3492.
4 A. You, M. A. Y. Be and I. In, On the optical band gap of zinc oxide, *J. Appl. Phys.*, 1998, **83**(10), 5447.
5 P. K. Stoimenov, R. L. Klinger, G. L. Marchin and K. J. Klabunde, Metal Oxide Nanoparticles as Bactericidal Agents, *Langmuir*, 2002, **18**(17), 6679–6686.
6 M. Roselli, A. Finamore, I. Garaguso, M. S. Britti and E. Mengheri, Biochemical and Molecular Actions of Nutrients Zinc Oxide Protects Cultured Enterocytes from the Damage Induced by Escherichia coli 1, *J. Nutr.*, 2003, **133**(12), 4077–4082.
7 J. Chellappa, Green synthesis of ZnO nanoparticles using Phyllanthus embilica stem extract and their antibacterial activity Green synthesis of ZnO Nanoparticles using Phyllanthus embilica Stem extract and their Antibacterial activity, *Der Pharm. Lett.*, 2018, **8**(11), 218–223.
8 Y. Gao, D. Xu, D. Ren, K. Zeng and X. Wu, Green synthesis of zinc oxide nanoparticles using Citrus sinensis peel extract and application to strawberry preservation: A comparison study, *LWT*, 2020, **126**, 109297.
9 P. A. Luque, *et al.*, Green synthesis of zinc oxide nanoparticles using Citrus sinensis extract, *J. Mater. Sci. Mater. Electron.*, 2018, **29**(12), 9764–9770.
10 O. J. Nava, *et al.*, Fruit peel extract mediated green synthesis of zinc oxide nanoparticles, *J. Mol. Struct.*, 2017, **1147**, 1–6.
11 A. Vahidi, H. Vaghari, Y. Najian, M. J. Najian and H. Jafarizadeh-Malmiri, Evaluation of three different green fabrication methods for the synthesis of crystalline ZnO nanoparticles using Pelargonium zonale leaf extract, *Green Process. Synth.*, 2019, **8**(1), 302–308.
12 S. Jafarirad, M. Mehrabi, B. Divband and M. Kosari-Nasab, Biofabrication of zinc oxide nanoparticles using fruit extract of Rosa canina and their toxic potential against bacteria: A mechanistic approach, *Mater. Sci. Eng. C*, 2016, **59**, 296–302.
13 S. B. Jaffri and K. S. Ahmad, Foliar-mediated Ag:ZnO nanophotocatalysts: Green synthesis, characterization, pollutants degradation, and in vitro biocidal activity, *Green Process. Synth.*, 2019, **8**(1), 172–182.
14 M. Zare, *et al.*, Novel Green Biomimetic Approach for Synthesis of ZnO-Ag Nanocomposite; Antimicrobial Activity against Food-borne Pathogen, Biocompatibility and Solar Photocatalysis, *Sci. Rep.*, 2019, **9**(1), 1–15.
15 G. M. J. Fowsiya, I. V. Asharani, S. Mohapatra, A. Eshapula, P. Mohi, N. Thakar, S. Monad and G. Madhumitha, Aegle marmelos phytochemical stabilized synthesis and characterization of ZnO nanoparticles and their role

against agriculture and food pathogen, *Green Process. Synth.*, 2019, **8**(1), 488–495.

16 G. Sharmila, M. Thirumarimurugan and C. Muthukumaran, Green synthesis of ZnO nanoparticles using Tecoma castanifolia leaf extract: Characterization and evaluation of its antioxidant, bactericidal and anticancer activities, *Microchem. J.*, 2019, **145**, 578–587.

17 N. Ain Samat and R. Md Nor, Sol-gel synthesis of zinc oxide nanoparticles using Citrus aurantifolia extracts, *Ceram. Int.*, 2013, **39**(SUPPL.1), 1–4.

18 F. Davar, A. Majedi and A. Mirzaei, Green synthesis of ZnO nanoparticles and its application in the degradation of some dyes, *J. Am. Ceram. Soc.*, 2015, **98**(6), 1739–1746.

19 M. Ramesh, M. Anbuvannan and G. Viruthagiri, Green synthesis of ZnO nanoparticles using Solanum nigrum leaf extract and their antibacterial activity, *Spectrochim. Acta, Part A*, 2014, **136**(B), 864–870.

20 S. O. Ogunyemi, *et al.*, Green synthesis of zinc oxide nanoparticles using different plant extracts and their antibacterial activity against Xanthomonas oryzae pv. oryzae, *Artif. Cells, Nanomedicine, Biotechnol.*, 2019, **47**(1), 341–352.

21 A. M. Awwad, M. W. Amer, N. M. Salem and A. O. Abdeen, Green synthesis of zinc oxide nanoparticles (ZnO-NPs) using Ailanthus altissima fruit extracts and antibacterial activity, *Chem. Int.*, 2020, **6**(3), 151–159.

22 N. Verma, S. Bhatia and R. K. Bedi, Role of pH on electrical, optical and photocatalytic properties of ZnO based nanoparticles, *J. Mater. Sci. Mater. Electron.*, 2017, **28**(13), 9788–9797.

23 P. S. Kumar, *et al.*, Biodegradability study and pH influence on growth and orientation of ZnO nanorods via aqueous solution process, *Appl. Surf. Sci.*, 2012, **258**(18), 6765–6771.

24 M. Pudukudy, A. Hetieqa and Z. Yaakob, Synthesis, characterization and photocatalytic activity of annealingdependent quasi spherical and capsule like ZnO nanostructures, *Appl. Surf. Sci.*, 2014, **319**(1), 221–229.

25 K. Shingange, Z. P. Tshabalala, B. P. Dhonge, O. M. Ntwaeaborwa, D. E. Motaung and G. H. Mhlongo, 0D to 3D ZnO nanostructures and their luminescence, magnetic and sensing properties: Influence of pH and annealing, *Mater. Res. Bull.*, 2017, **85**, 52–63.

26 H. Çolak and E. Karaköse, Green synthesis and characterization of nanostructured ZnO thin films using Citrus aurantifolia (lemon) peel extract by spin-coating method, *J. Alloys Compd.*, 2017, **690**, 658–662.

27 N. A. Salahuddin, M. El-kemary and E. M. Ibrahim, "Synthesis and Characterization of ZnO Nanoparticles via Precipitation Method: Effect of Annealing Temperature on Particle Size, *Nanosci. Nanotechnol.*, 2015, **5**(4), 82–88.

28 N. Bala, *et al.*, RSC Advances Green synthesis of zinc oxide nanoparticles using Hibiscus subdariffa leaf extract: Effect of temperature on synthesis, anti-bacterial activity and anti-diabetic activity, *RSC Adv.*, 2015, **5**(7), 4993–5003.

29 G. Madhumitha, J. Fowsiya, N. Gupta, A. Kumar and M. Singh, Graphical abstract SC, *J. Phys. Chem. Solids*, 2019, **127**, 43–51.

30 X. Tong, H. Zhang and D. Y. Li, Effect of Annealing Treatment on Mechanical Properties of Study, *Sci. Rep.*, 2015, **5**(1), 1–7.

31 B. Zapata, J. Balmaseda, E. Fregoso-Israel and E. Torres-García, Thermo-kinetics study of orange peel in air, *J. Therm. Anal. Calorim.*, 2009, **98**(1), 309–315.

32 I. M. Alibe, *et al.*, EFfects of calcination holding time on properties of wide band gap willemite semiconductor nanoparticles by the polymer thermal treatment method, *Molecules*, 2018, **23**(4), 1–18.

33 I M McIntosh, A. R. L. Nichols, K. Tani and E. W. Llewellin, Accounting for the species-dependence of the 3500 cm^{-1} H_2Ot infrared molar absorptivity coefficient: Implications for hydrated volcanic glasses, *Am. Mineral.*, 2017, **102**(8), 1677–1689.

34 O. Yamamoto, Influence of particle size on the antibacterial activity of zinc oxide, *Int. J. Inorg. Mater.*, 2001, **3**(7), 643–646.

35 S. B. Shetty, P. Mahin-syed-ismail, S. Varghese, B. Thomas-george and P. Kandathil-, "Antimicrobial effects of Citrus sinensis peel extracts against dental caries bacteria: An in vitro study, *Journal of Clinical and Experimental Dentistry*, 2016, **8**(1), e70–7.

36 L. Zhang, *et al.*, Mechanistic investigation into antibacterial behaviour of suspensions of ZnO Mechanistic investigation into antibacterial behaviour of suspensions of ZnO nanoparticles against *E. coli*, *J. Nanoparticle Res.*, 2010, **12**(5), 1625–1636.

37 M. J. Chithra and M. S. K. Pushpanathan, Effect of pH on Crystal Size and Photoluminescence Property of ZnO Nanoparticles Prepared by Chemical Precipitation Method, *Acta Metall. Sin. (Engl. Lett.)*, 2015, **28**(3), 394–404.

38 H. Padalia, S. Baluja and S. Chanda, Effect of pH on Size and Antibacterial Activity of Salvadora oleoides Leaf Extract-Mediated Synthesis of Zinc Oxide Nanoparticles, *Bionanoscience*, 2017, **7**(1), 40–49.

39 A. Lipovsky, Z. Tzitrinovich, H. Friedmann, G. Applerot, A. Gedanken, R. Lubart, *et al.*, EPR Study of Visible Light-Induced ROS Generation by Nanoparticles of ZnO, *J. Phys. Chem. C*, 2009, **113**(36), 15997–16001.

40 A. Sirelkhatim, S. Mahmud and A. Seeni, "Review on Zinc Oxide Nanoparticles: Antibacterial Activity and Toxicity Mechanism, *Nano-Micro Lett.*, 2015, **7**(3), 219–242.

41 A. Lipovsky, A. Gedanken and R. Lubart, "Antifungal activity of ZnO nanoparticles – The role of ROS mediated cell injury, *Nanotechnology*, 2011, **22**(10), 105101.